mathematics

MDPI

Article

Novel Approach of Airfoil Shape Representation Using Modified Finite Element Method for Morphing Trailing Edge

Martynas Lendraitis * and Vaidas Lukoševičius

Faculty of Mechanical Engineering and Design, Kaunas University of Technology, Studentų Str. 56, 51424 Kaunas, Lithuania

* Correspondence: martynas.lendraitis@ktu.lt

Abstract: This study presents a novel approach to parameterize the geometry of a morphing trailing-edge flap that allows its aerodynamics to be optimized while capturing the expected structural behavior of the flap. This approach is based on the finite frame element method, whereby the initial flap surface is defined as a structure with constraints that are similar to those of a morphing flap with passive skin. The initial shape is modified by placing a series of distributed loads on the surface. The finite frame element method is modified with rigid rotation corrections to maintain the initial element length without requiring nonlinear calculations and to achieve accurate surface-length results by only solving the linear FEM equations twice. The proposed method enables the shape of the morphing flaps to be rapidly formulated while maintaining the initial upper surface-length and trailing-edge angle. The constraints are inherently integrated into the algorithm, eliminating the need for unnecessary feasibility checks during the aerodynamic optimization. By using the proposed airfoil parameterization method, a case study was conducted by using a genetic algorithm to optimize the lift-to-drag ratio of the NACA 23012 airfoil flap starting at 0.7c with 10 degrees of deflection. The optimizer resulted in a structurally feasible morphing flap that achieved a 10% increase in the lift-to-drag ratio in the optimized angle of attack range.

Keywords: airfoil parametrization; morphing wing; trailing edge

MSC: 65D99; 76M10; 49Q10

check for updates

Citation: Lendraitis, M.; Lukoševičius, V. Novel Approach of Airfoil Shape Representation Using Modified Finite Element Method for Morphing Trailing Edge. *Mathematics* **2023**, *11*, 1986. https://doi.org/10.3390/math11091986

Academic Editor: Hong Zheng

Received: 20 March 2023
Revised: 7 April 2023
Accepted: 22 April 2023
Published: 23 April 2023

Copyright: © 2023 by the authors. Licensee MDPI, Basel, Switzerland. This article is an open access article distributed under the terms and conditions of the Creative Commons Attribution (CC BY) license (https://creativecommons.org/licenses/by/4.0/).

1. Introduction

Morphing wing technology has attracted considerable attention in the field of aerospace engineering due to its ability to increase the flight performance of an aircraft. Implementing continuous trailing edge morphing in a commercial aircraft can result in a 2.7% reduction in fuel burn when considering the entire mission envelope [1]. Furthermore, the presence of a morphing flap on a wing can help reduce the broadband-noise level by up to 11% compared with a conventional single-slot flap [2]. When investigating the performance of 2D airfoils, a morphing wing trailing-edge flap can help increase the L/D ratio by up to 18.7% [3] and provide a higher lift for the same deflection angle. Clearly, morphing flaps are superior to conventional flap configurations. One of the most important aspects of developing morphing wings is finding an effective method to parameterize the airfoil shape to perform an aerodynamic optimization. The parameterization of the airfoil shape has a considerable impact on the optimization of the results because it needs to accurately represent the shape of the airfoil [4].

Multiple different methods can be used to describe the shape of an airfoil, such as B-splines, PARSEC, class, and shape function transformation (CST), and others. These methods have been thoroughly investigated and compared with each other by several authors [4–6]. The B-spline has gained popularity in airfoil shape representation due to its versatility and ease of use. The B-spline is a piecewise polynomial curve represented by a

set of control points. The curve is defined as a weighted sum of the basis function with the weighting values of the control points. Airfoil shapes represented with B-splines can be easily and intuitively modified by changing the location of the control points.

The PARSEC method [7] was specifically developed to generate airfoils, and the method entails the use of defined geometric airfoil parameters to control the shape. The airfoil is then described by using a linear combination of shape functions. This method is intuitive because the used parameters are tied to the physical airfoil geometry.

Currently, the CST method introduced by Kulfan [8] is the most popular method. Its use produces smooth geometries and provides a high degree of control over the airfoil geometry, which makes it easier to fine tune the shape to obtain an optimal design. This method consists of a class and shape function. The class function defines the fundamental shape of the airfoil with a round leading edge and sharp trailing edge. The shape function is used to alter the overall geometry of the airfoil. Compared with the PARSEC method, the CST method can be used to handle more complex shapes and allows for smooth transitions between different airfoil sections. Several extensions have recently been added to the CST method, such as in [9] whereby the authors achieved an increase in accuracy and a reduction in the minimal number of control points. Further developments of the original CST have not only increased the precision of the CST method but have also caused it to be more intuitive, as presented in [10,11]. The latter study developed the intuitive CST model further by enabling section decoupling, which allowed for even more effective parameterization. Feng [12] suggests adding additional variables from linearized aerodynamic theory. These methods are widely used in practice to optimize conventional and morphing airfoils.

There are two types of morphing skin: active skin, which allows for extension and compression as well as bending, and passive skin, which can only be bent. Typically, designed morphing structures have the ability to extend the structure skin, either by using some form of polymer skin that is flexible and covers the entire structure [13,14], or by having mechanical overlapping skin [15,16]. These studies hold considerable significance in the field due to the high complexity of fully morphing structure where the shape needs to change significantly. These approaches do not require specialized airfoil shape representation methods, as no accurate skin length control is needed. Unfortunately, morphing-compliant structures require the skin length to be controlled with addition to the other constraints, where previously mentioned shape representation methods do not directly provide, and thus they require additional modifications to their algorithm. Topology optimized morphing structures are often created with passive skin [17–21]. Therefore, optimizing the aerodynamic shape of such structures is more complex, as it requires additional feasibility checks.

De Gaspari [22] proposed a modified CST method that involves using an iterative process to control the skin length and other parameters by using the single-value optimization and curve-fitting technique to achieve the desired wing shape without changing the surface-skin length. Leal [23] investigated the morphing wing with camber morphing parameterization, while considering the internal-structure kinematics, and provided a structurally consistent CST formulation with the use of active or passive skin. Although these methods are accurate, they require the allocation of additional computational resources and may be difficult to implement.

With this paper, a new approach that is based on the finite beam element method is presented, which allows to capture the behavior of the physical structure during aerodynamic optimization, mostly by constraints which are inherently integrated in the structural algorithm. By incorporating the finite frame element method, the length of the skin can be effectively preserved, ensuring that the optimized airfoil geometry adheres to the necessary constraints. This method is based on the linear calculation of finite element beams with a modification that corrects for the resulting skin-length inaccuracies in linear calculation. With this method, the main constraints are preimposed on the generated shape through structural integrity, which eliminates unnecessary feasibility checks. This method requires linear equations to only be solved twice without the need to iterate; therefore, this method is not computationally intensive and is suitable for fast optimization problems.

This paper consists of the following sections: the introduction, shape representation methodology, FEM modifications, initial shape, case study, and discussions.

2. Shape Representation Methodology

Incorporating the morphing structure behavior of a trailing edge when optimizing an aerodynamic shape is highly desirable. This allows only feasible shape designs to be evaluated during optimization without the need for feasibility testing which reduces the optimization time. One way to accomplish this is to represent the trailing edge structure of the airfoil as a frame structure and to alter the shape by applying external loads. In this section, the proposed methodology is described.

An initial shape that represents the arbitrary morphed trailing edge section of the airfoil with a desired flap deflection y_p (Figure 1) must first be defined. The shape is then converted into a structure that is divided into a set of finite frame elements. Because the method is used to represent flap shapes with a morphing-compliant structure, the modeled structure must have boundary conditions that are similar to those of the morphing structure.

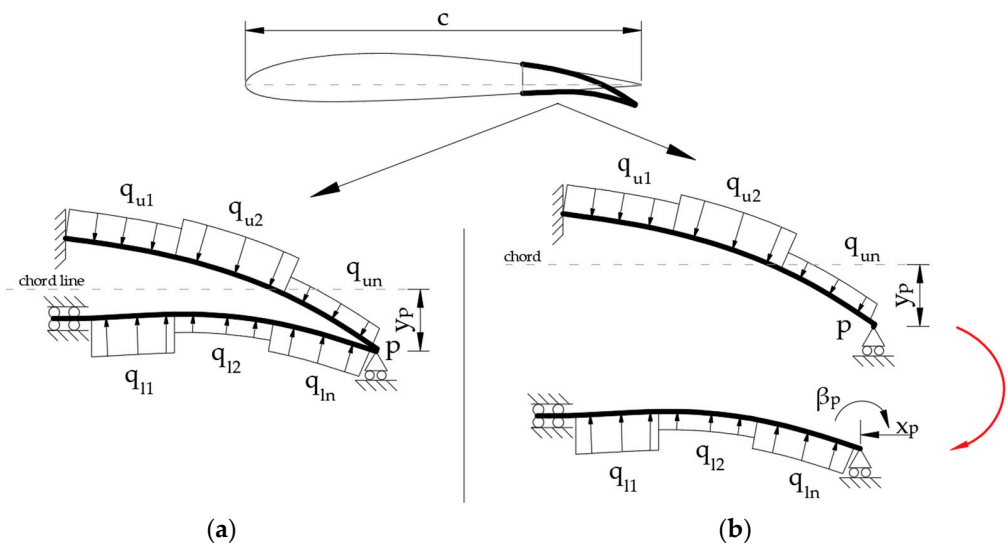

Figure 1. Trailing-edge flap optimization setup with defined boundary conditions: (**a**)—top and bottom surface are coupled; (**b**)—top and bottom surface are decoupled (used in analysis).

The upper skin forward section is rigidly connected to the front section of the airfoil, which imposes a tangential constraint on the rest of the airfoil. The forward section of the lower surface must have a sliding joint, which is common in this type of compliant morphing design and represents stretchable skin. To ensure a tangential constraint with the rest of the airfoil section, the surface must be able to move along the forward airfoil surface. Finally, the trailing edge node p should be constrained to the desired deflection position y_p. The node should only be constrained in the vertical direction and allow for rotation and longitudinal motion along the chord to capture the chord length reduction as the morphed flap curves. All the mentioned constraints are shown in Figure 1.

Figure 1a shows continuous structure-morphing flap arrangement. In such an arrangement, the forces applied to the upper surface will have an effect on the lower surface. This might not be particularly useful for shape optimization. The coupling between two surfaces might reduce the optimizer performance and increase the objective function evaluation count to reach the optimal solution. When the applied loads change on the upper or lower surface, they globally affect the whole shape, making the optimization sensitive to all the individual parameters. Therefore, in order to solve the optimization problem, a higher population number might be needed. The upper and lower surfaces can be decoupled to obtain the independent behavior of the upper surface (Figure 1b). In such a case, the calculation is first performed on the top surface, using the constraints mentioned above.

Then, the resulting translation x_p and rotation β_p at the trailing-edge node are used as a boundary condition for the lower surface calculation. This causes the top surface to be independent, while the bottom surface continues to be affected by the initial displacement of the trailing-edge node caused by the upper surface displacement. When using both methods, the trailing-edge angle is largely preserved. The decoupled approach (Figure 1b) is more preferred when optimizing airfoils flaps because it may converge faster. Therefore, we employed this approach further.

The initial flap shape is modified by adjusting a set of discrete, equally spaced, distributed loads, denoted as q_n, that are applied to the flap surface, where $q_{l1\ldots n}$ is for lower surface and $q_{u1\ldots n}$ for top surface. These loads are treated as variables in the optimization problem and vary from −1 to 1 N/m. To achieve the desired shape alteration, the stiffness of the structure must be adjusted accordingly so that the shape boundaries can be obtained. Shape behaviors can be defined by the maximum structural deflection when the maximum load of all the variables is applied. A straight homogeneous cantilever beam with a supported end (Figure 2) will closely approximate the structural behavior of the top surface of the morphing flap, which have the same length L between the supports. The application of a continuously distributed load of q = 1 N/m on the surface represents the maximum loading and allows to calculate the normalized stiffness value for a defined maximum total deflection y_{max}. The approximated analytical expression for the normalized stiffness is then defined:

$$EI_n = \frac{2L^4}{369y_{max}} \tag{1}$$

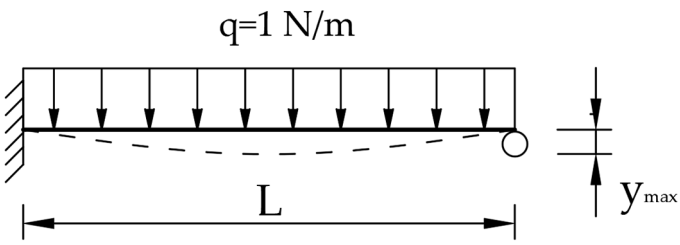

Figure 2. Boundary conditions of a straight homogeneous beam with constant distributed loading.

Due to the possible curvature of the initial airfoil shape, the approximation may not be highly accurate. The normalized bending stiffness can also be iteratively determined on the curved airfoil structure before starting the optimization. Thus, more accurate maximum deformation boundaries can be achieved. However, the authors think that such a determination is unnecessary in most cases unless strict shape optimization bounds are needed.

The AE_n value of axial stiffness is arbitrary as it does not contribute to the final shape because there is no axial loading. During the modified FEM calculation, an additional artificial force is introduced to correct the length of the element at large deformations. Therefore, it is necessary to include the axial-stiffness values to ensure accurate results. More details are described in the next chapter.

After the deformed structure is obtained, the node coordinates are joined with the rigid airfoil section coordinates, so that the aerodynamic calculation on a new airfoil can be performed.

The summary of the described method for formulating the airfoil trailing edge shape in a context of airfoil optimization can be represented by the algorithm shown in Figure 3.

The algorithm begins by initializing the initial shape which will eventually be morphed into the final geometry. This initial shape can be arbitrary or defined numerically. The implementation of the initial shape is described in Section 4. Based on the defined initial structure dimensions, the normalized stiffness parameters are calculated. Then the structure is discretized to finite elements and boundary conditions are applied. As a means of optimization, loading values are introduced to control the shape, which are generated by the optimizer. At this stage, the optimization loop starts. After structural evaluation, new morphed shape coordinates are determined which are joined with the coordinates of

the rigid section of the airfoil to form the complete airfoil coordinate set. After that, the aerodynamic performance can be evaluated. The optimizer iterates through multiple cycles until it converges on a solution.

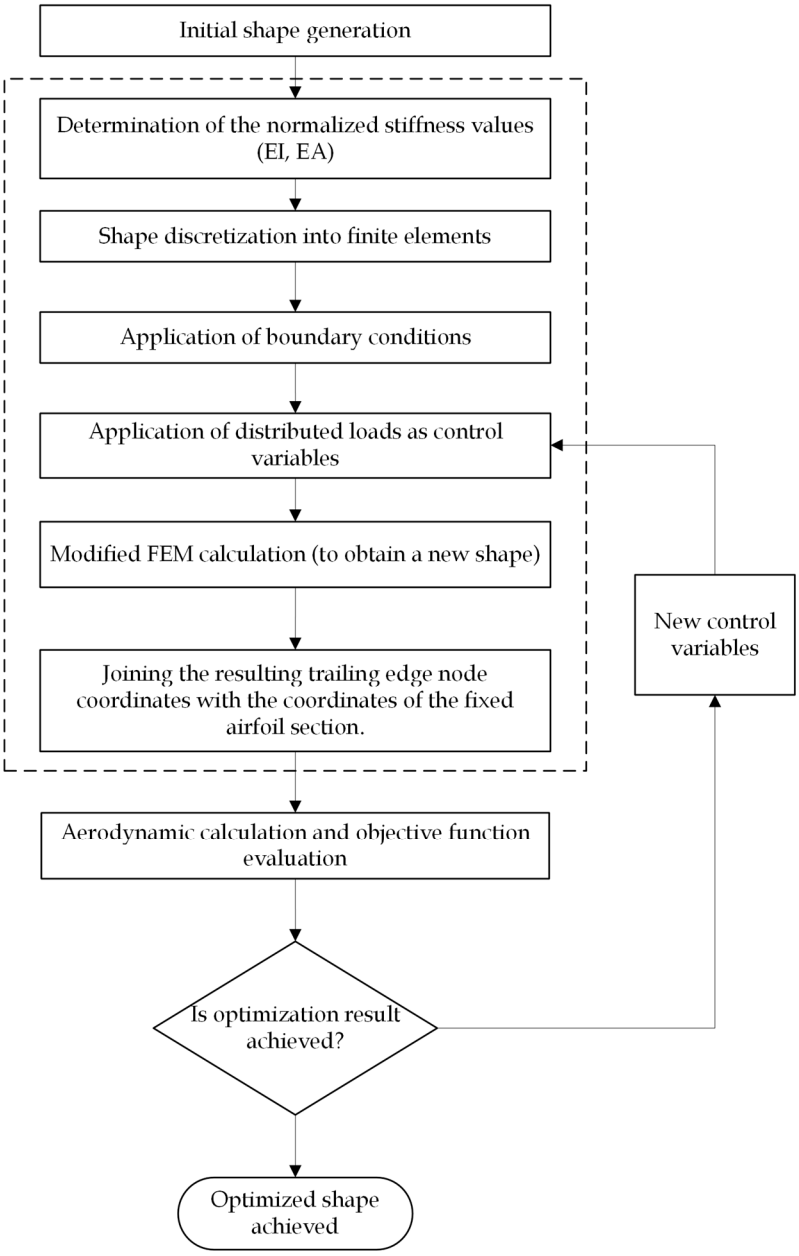

Figure 3. Shape representation algorithm in context of airfoil optimization. The shape alteration sequence is encircled with a dashed line.

3. FEM Modifications

The airfoil section geometry can be effectively modeled with existing FEM algorithms without requiring additional modifications. However, to accurately represent the geometry at large deformations, a computationally-intensive nonlinear solver must be used. Although direct structural modeling might be used in fluid structure interaction studies, when examining behavior in between structure and the flow, it is rarely utilized in direct aerodynamic optimization when representing airfoil shapes due to large computational cost. Using a linear FEM method is more efficient and more suitable for such a purpose. However, using a fully linear calculation is not feasible in shape representation, as it results in a deformed shape at high deformations as the physical element size changes. We propose

a modification of the finite element algorithm for planar frames that corrects the results of the initial linear calculations with the necessary corrections required to maintain the initial element length while keeping the computation time short.

Frame element analysis is a method that is commonly used to represent planar structures when conducting a linear structural analysis. With this method, the properties of a beam and truss are combined according to the superposition principle. Whereas a truss only deforms in the axial direction, the main cause of planar shape distortions comes from the beam element. The beam element only allows for transverse deflection and neglects any resulting axial displacement, which thus artificially expands the element. To represent the beam deflection behavior, the Euler–Bernoulli method is often used. The Euler–Bernoulli equation shows the relationship between the beam's deflection and the applied loads. The differential equation for a beam with constant rigidity is written as [24]:

$$EI\frac{d^4w}{dx^4} = q(x) \tag{2}$$

where w is the deflection, q(x) is the distributed load along the beam, and EI is the bending stiffness.

The assumption of Bernoulli's equation is that the section plane remains perpendicular to the normal axis. In a linear formulation, the deformations are assumed to be small enough to allow for small angle approximations. Therefore, the beam deflection angle θ can be approximated:

$$\theta(x) \approx \frac{dw}{dx} \tag{3}$$

This results in the further approximation that the cosine of θ is approximately equal to one and that no variations in length along the local element *x*-axis exist, whereas the element deflects in the transverse direction and artificially expands the element. Although this assumption is well regarded in structural calculations, when deformations are small, such assumptions are not valid when expecting larger deformations, as it results in structure distortion and poor accuracy.

When avoiding the utilization of computationally expensive nonlinear calculations, nonphysical considerations can be applied if the geometrical deformation accuracy is not critical. These considerations assume that the beam has a rigid rotation and maintains its physical length after deflection. By knowing the element deflection, the difference between the initial and deformed element length can be calculated and later corrected.

Figure 4 shows a simplified drawing of a beam element with length L_e after deformation in the local coordinate system. The figure only shows element rotation along the first node, used as a reference. As can be seen, no change in the length in the local *x*-axis occurred after the element deformation; therefore, the actual element length was stretched by δ and the total element length increased. To incorporate the adjustments, the projected reduction in the local *x*-axis due to rigid rotation needs to be determined. When the transverse deflection value v_e is known and is maintained, the projected element shortening in the local x axis can be determined:

$$\Delta_e = L_e - \sqrt{L_e^2 - v_e^2} \tag{4}$$

As can be seen in Figure 4, the deflection angle θ'_e is different from the one determined initially θ_e.

Here, using frame elements offers the benefit of having an additional independent degree of freedom, which can be used to impose the corrections as a means of axial force. This axial force $F_{add.e}$ needs to shorten the beam element when deflection occurs so that the beam end node aligns with the rightly rotated beam node location; this preserves the displacement value, which is obtained after the initial calculation. By knowing Δ_e distance

and the axial stiffness of the beam element, the correcting axial force is calculated using the following equation:

$$F_{add.e} = \frac{\Delta_e E A_n}{L_e} \tag{5}$$

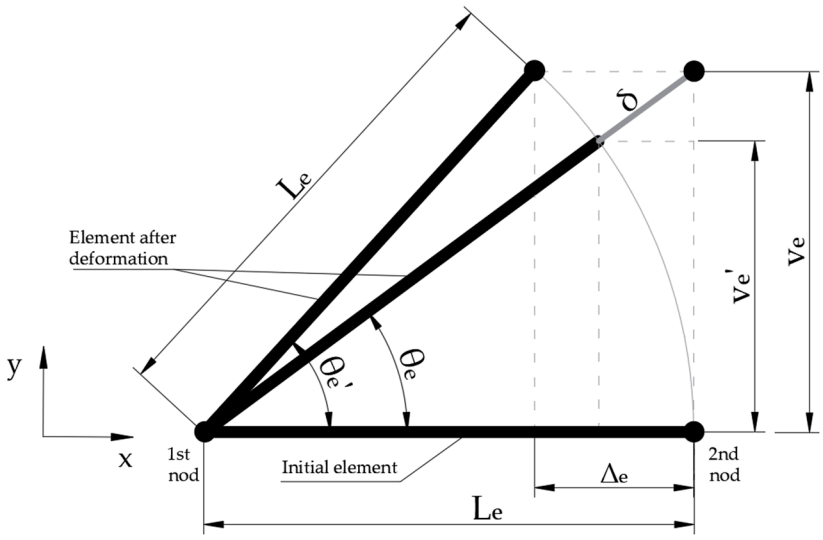

Figure 4. Distorted and corrected beam element after deflection in local element coordinate system. Total deflection is shown in reference to the first node.

This approach requires at least two linear FEM calculations. During the second iteration, the additional force is added to the initial beam boundary conditions, and the calculations are re-evaluated. The resulting node location will now be in line with the rigidity rotated beam, and the initial element length will be preserved.

This approach is feasible when the structure is not highly constrained and has some possibility of movement. However, when the beam is fully constrained at both ends, the beam length may not be accurately calculated.

The described method can be easily incorporated into a traditional frame calculation routine, similar to the one explained in reference [25]. The frame element has six degrees of freedom, as shown in Figure 5. The element displacement vector d_e is formulated in the following manner:

$$d_e = \begin{bmatrix} u_{e1} & v_{e1} & \theta_{e1} & u_{e2} & v_{e2} & \theta_{e2} \end{bmatrix}^T \tag{6}$$

where u_{e1},u_{e2} are the longitudinal displacement of the element node, v_{e1},v_{e2} are the transverse displacement, and θ_{e1},θ_{e2} are the rotation of the node.

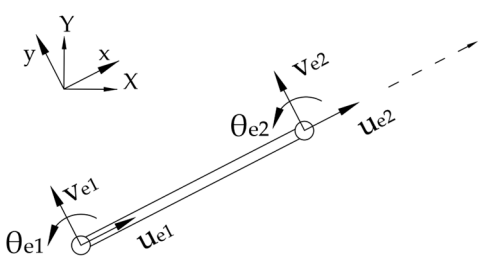

Figure 5. Frame element in the global coordinate system with degrees of freedom shown in local coordinate system.

The element stiffness matrix k_e is defined in the same way as in the mentioned reference, except that it required normalized bending EI_n, and axial stiffness EA_n.

$$k_e = \begin{bmatrix} \frac{EA_n}{L_e} & 0 & 0 & -\frac{EA_n}{L_e} & 0 & 0 \\ 0 & 12\frac{EI_n}{L_e^3} & 6\frac{EI_n}{L_e^2} & 0 & -12\frac{EI_n}{L_e^3} & 6\frac{EI_n}{L_e^2} \\ 0 & 6\frac{EI_n}{L_e^2} & 4\frac{EI_n}{L_e} & 0 & -6\frac{EI_n}{L_e^2} & 2\frac{EI_n}{L_e} \\ -\frac{EA_n}{L_e} & 0 & 0 & \frac{EA_n}{L_e} & 0 & 0 \\ 0 & -12\frac{EI_n}{L_e^3} & -6\frac{EI_n}{L_e^2} & 0 & 12\frac{EI_n}{L_e^3} & -6\frac{EI_n}{L_e^2} \\ 0 & 6\frac{EI_n}{L_e^2} & 2\frac{EI_n}{L_e} & 0 & -6\frac{EI_n}{L_e^2} & 4\frac{EI_n}{L_e} \end{bmatrix} \tag{7}$$

During the initial calculation, the force vector only contains values from the distributed loading $q_{e.i}$ that were transferred from the shape control variables to the corresponding elements, which are necessary to alter the airfoil shape:

$$f_e = \begin{bmatrix} 0 & \frac{q_{e.i}L_e}{2} & \frac{q_{e.i}L_e^2}{12} & 0 & \frac{q_{e.i}L_e}{2} & -\frac{q_{e.i}L_e^2}{12} \end{bmatrix}^T \tag{8}$$

Before assembling the full structural matrix, coordinate transformations are per-formed for each element. Once the global matrix is assembled, the boundary conditions are applied by removing the corresponding rows and columns from the stiffness matrix and force vector. The following form of linear equations is solved to obtain the deformation vector:

$$\mathbf{KD} = \mathbf{F} \tag{9}$$

where **K** is the global stiffness matrix, **D** is displacement vector and **F** is the force vector.

After determining the initial nodal displacements of each element, the system is prepared for the second iteration by calculating the total transverse deflection for every element:

$$v_{e2} - v_{e1} = v_e \tag{10}$$

The additional correcting force for each element can be calculated using Equation (5). The calculated forces exerted on all the elements are applied on both element nodes and are directed in the opposite direction toward the element center along the local *x*-axis. Thus, this only axially affects the element. Then, during the second calculation, the element force vector becomes:

$$f_e = \begin{bmatrix} F_{add.e} & \frac{q_{e.i}L_e}{2} & \frac{q_{e.i}L_e^2}{12} & -F_{add.e} & \frac{q_{e.i}L_e}{2} & -\frac{q_{e.i}L_e^2}{12} \end{bmatrix}^T \tag{11}$$

During the second calculation, the stiffness matrix does not need to be reassembled, and its initial form can be used. Once again, solving Equation (9) with the new force vector provides corrected nodal displacements, where the initial length of the beam element is consistent with the rigid rotation and the initial length of the elements are unchanged.

In summary, the described FEM modification made to maintain the initial element length can be represented by the calculation sequence algorithm presented in Figure 6.

Although this method can be used to effectively preserve the initial length of the structure after deformations, errors can still occur when using it. Some errors arise from the discretization and from the described model itself. The elements from the discretization error, representing a curved shape, will quickly become negligible if a reasonable number of elements are used.

Taking into account the errors caused by the proposed method, for a straight beam with boundary conditions as shown in Figure 2, the total sum of all element lengths after deformation is accurately preserved up to an element rotation of almost 90 degrees. However, if the investigated beam has curvature, the structure is somewhat more constrained and additional errors may occur. Such errors arise due to axial constraints at both beam ends.

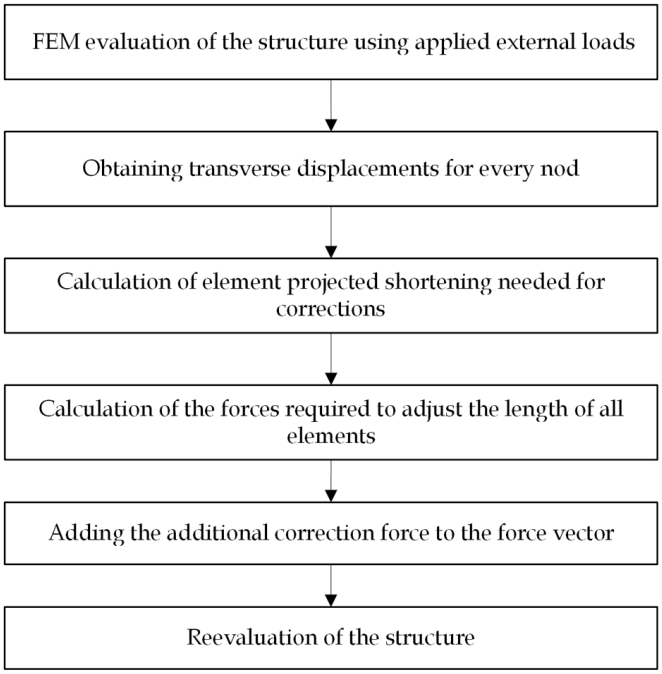

Figure 6. Modified FEM algorithm initiation sequence.

However, when this method is employed for airfoil optimization, the resulting length error is negligible. For example, when examining the top surface of an airfoil flap, as shown in Figure 1, the error in the sum of all the element lengths after deformation does not exceed 5×10^{-7}%, with maximum deflections corresponding to 1/10th of the surface length. Such a deformation is usually larger than that used during a typical flap optimization.

4. Initial Shape

This method requires an initial shape representing the structure to serve as the basis for optimization. All the initial constraints, such as the surface length and trailing-edge angle, must be respected at the specified deflection of the flap optimization. For a compliant morphing trailing edge, the top surface is passive and its length does not change during morphing. However, the bottom-surface length does change and the amount will depend on the final geometry. Although the initial structure can be arbitrarily defined, having a consistent method to define it is convenient.

For this purpose, a structural calculation to obtain the shape can be used by using the fully nonlinear calculation or the modified finite-element method described above. The undeformed trailing-edge section must be defined as a structure and divided into a set of finite elements. Following the earlier description, boundary conditions similar to those encountered on the compliant trailing edge with morphing must be applied to the structure, as shown in Figure 7. To impose deflection on a morphing flap, a prescribed deflection is applied to the trailing-edge node. No other forces are applied to the calculation. Then, the finite element equations are solved, and the deformed shape is determined. Because the stiffness values are constant along the structure, the deformed structure results in a smooth curve that strongly resembles a morphed flap.

The length of the upper surface of the flap is unchanged, whereas the lower surface shifts along the slider joint. This results in a reduction in the lower-surface length, as would be expected with such a morphing structure. To present the final initial structure, an additional adjustment is made. As the surface moves toward the leading edge, the constrained nodes move together. Therefore, the structure at the starting position of the flap may also shift in the y direction. This shift is usually minor and can be ignored. However, to achieve a smooth transition with an unmorphed airfoil section, an additional adjustment can be made. To perform the necessary adjustment, the bottom surface is trimmed at the

sliding-joint location, excluding the excess curve. Then, the new boundary conditions are applied with the top surface fully constrained at the starting point and supported only at the trailing edge, whereas the bottom leading portion remains unconstrained. Finally, the defined displacement is applied to the end of the curve, which corresponds to the desired displacement in the y direction. The resulting shape can then be used as the initial structure for optimization described in the paper.

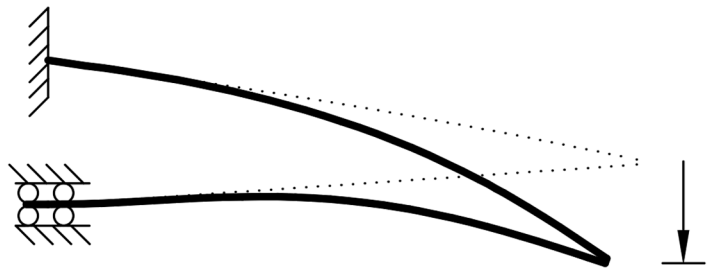

Figure 7. Initial airfoil structure and its boundary conditions. The prescribed displacement is defined at the trailing edge.

5. Case Study

The objective of this case study was to demonstrate the effectiveness of the proposed shape representation method. For this purpose, a MATLAB program was developed. To demonstrate the results, NACA 23012 was chosen for evaluation. The optimization process was carried out on the trailing edge section of the airfoil, starting from the chord-wise location of 0.7 and extending to the end of the trailing edge. The vertical displacement of the trailing edge of the flap was fixed and set to 0.05c, which corresponded to a flap deflection angle of approximately 10 degrees.

For the shape representation, the entire surface of the flap was discretized into 61 frame elements. As described in Section 2, the control points were defined as equally spaced distributed loads of a constant magnitude. A total of eight control points were defined to change the shape. The four control points were designated for the upper surface and the remaining four were designated for the lower surface. To approximate the design space, the bending stiffness was calculated using the expected deflection of y_{max} = 0.03, which was defined as the surface bounds for the analysis. The resulting bending stiffness value corresponded to $EI_n = 1.5 \times 10^{-3}$. The optimization bounds were defined by the deflection values for both positive and negative y_{max} values. Figure 8 shows the total design space for the upper and lower surfaces.

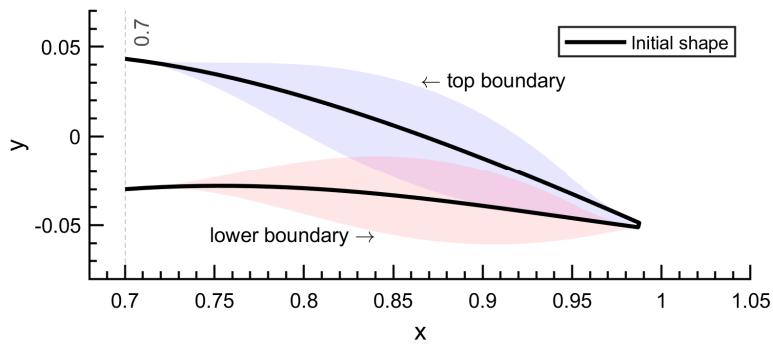

Figure 8. Initial structure and design space for top and bottom surfaces.

The aerodynamic performance was evaluated using the XFOIL software [26], a robust aerodynamic airfoil solver that is frequently used in airfoil optimization. Flap optimization was performed at a Reynolds number of 500,000. For each shape, a series of seven angles of attack between 0 and 6 degrees were evaluated. A larger number of angles of attack were investigated to determine the aerodynamic performance under a wide range of

conditions and to avoid localized optimization solutions that could result in bumps in the optimized shape [27].

To achieve the best aerodynamic performance, the objective function guiding the optimization was defined as the sum of the lift-to-drag coefficients obtained from all the evaluated angles of attack:

$$\text{maximize} \sum_{i=1}^{n} \frac{C_{l.i}}{C_{d.i}} \tag{12}$$

Due to the highly nonlinear nature of airfoil optimization and the existence of multiple possible solutions, the genetic algorithm is commonly chosen. Therefore, the optimization process in this case study was performed by using the integrated genetic algorithm in MATLAB [28], with a population size of 200 individuals. The optimization was completed after 50 generations and resulted in the best flap shape.

The optimized shape is compared with the conventional flap in Figure 9. As can be seen, the flap shapes differed from each other. In particular, the optimized shape had a more pronounced curvature and a retracted trailing edge. This retraction was considerably smaller in the conventional flap because the trailing edge followed the arc as it was rotated along the flap hinge. In contrast, when the morphing flap was deflected, the length of the upper surface was maintained, and the trailing edge was retracted even more. This retraction increased as the surface curvature increased. Additionally, the algorithm kept the trailing edge angle similar to the one in the initial structure, even without imposing additional constraints.

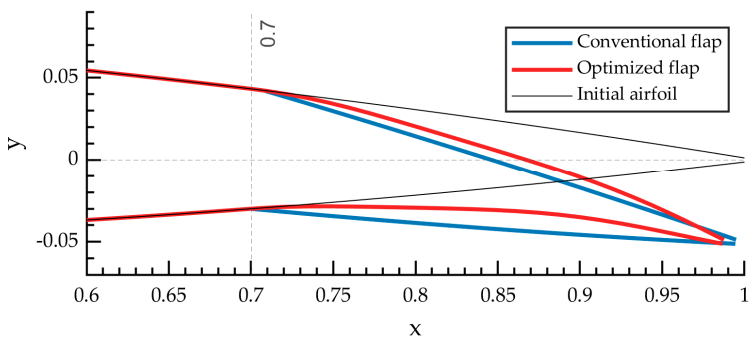

Figure 9. Geometry of the NACA 23012 trailing edge with the conventional and optimized flap.

When comparing the aerodynamic performance of the conventional and optimized flaps (Figure 10), the results showed an increase in the lift-to-drag ratio of about eight points (10%) in the optimized angle-of-attack range and significantly more at lower angles. Performance improvement at off-design angles of attack (mainly negative angles) can be primarily attributed to the increased smoothness of the morphing flap, particularly the elimination of sudden jump in curvature present in a conventional flap at the hinge mitigates possible flow separation.

The optimized flap had a smaller drag at the same lift coefficients. The highest performance increase was observed at small angles of attack, whereas at higher angles of attack the performance was almost the same. The optimized flap also increased the lift capability by increasing the maximum lift by 4.9%. A similar increase was observed at all angles of attack. These improvements demonstrate the advantage that can be achieved with a morphing flap, and they confirm the ability to use the proposed method to achieve much better performance. Additionally, the observed performance improvements align closely with the findings reported by other researchers [3,29,30].

It should be emphasized that the possible improvement due to the implementation of morphing flaps strongly depends on the initial airfoil, Reynolds number, and deflection angle. The presented case study is only one possible result, showing a great potential for morphing flap technology.

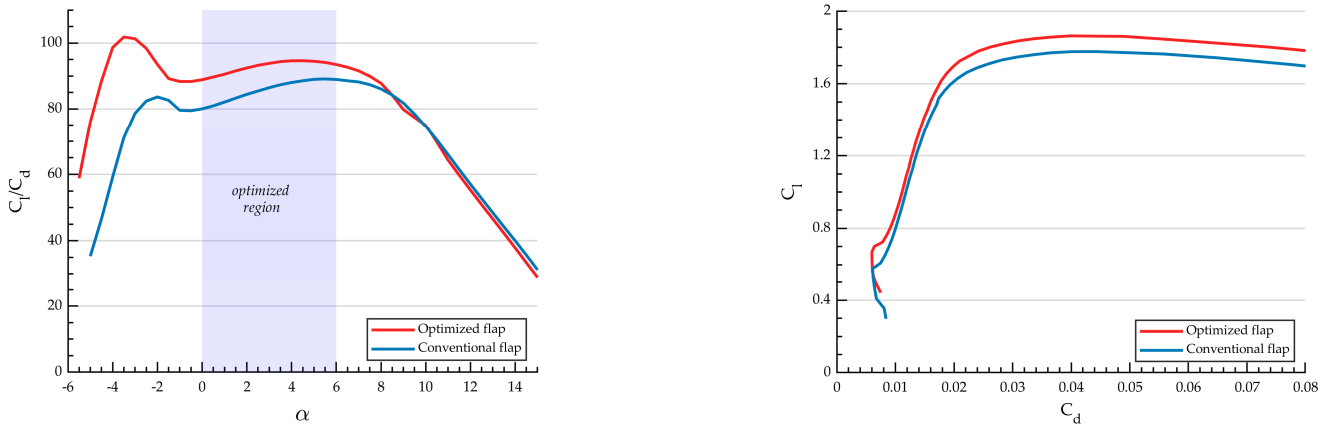

(**a**) (**b**)

Figure 10. Comparison of the performance of the conventional flap with the morphing flap: (**a**)—C_l/C_d dependence on the angle of attack α; (**b**)—relationship between lift (C_l) and drag coefficient (C_d), commonly referred to as a drag polar.

6. Discussion and Future Possibilities

The presented method is an efficient and intuitive method for representing the morphing trailing edge for aerodynamic optimization. Defining the surface morphing boundaries via maximum structural deflection is intuitive for the designer; doing this helps to define and link the morphing capabilities between the actual morphing structure and the flap-shape optimization.

The key advantage of the described shape representation method is the ability to maintain the initial length of the upper flap surface without needing to iterate. However, the true length of the surface will be affected by a discretization error which can be reduced by increasing the number of elements until the point of negligible error, which is in the scope of morphing the structure-morphing capabilities.

The second advantage of this method is the possibility to stiffen the structure in particular locations to maintain certain initial airfoil features. For example, stiffening the trailing-edge element or adding a cross-sectional member that joins the upper and lower skins can help maintain the trailing-edge angle through the optimization. This implementation does not increase the computational cost and helps to mitigate the possibility of generating a nonfeasible shape, which might waste calculation time.

The presented method could be extended in several ways to achieve specific results. For this work, the trailing-edge deflection was considered fixed. This is useful when optimizing the flap performance at a specific deflection angle. In some cases, the angle might not be known prior to optimization; therefore, the optimization should be set up in such a way that the flap deflection is added as one of the optimization variables. For such an optimization, the initial shape would have to be defined at every optimization run, thus increasing the computational cost. Such optimization might benefit from implementing multi-objective optimization strategies, where multiple conflicting objectives need to be assessed. A similar strategy is described in [31,32] where researchers use NSGA-II solver to obtain pareto front results. The optimization process can be configured to target specific objectives, such as maximizing the lift-to-drag ratio versus the change in lift for multiple designs. By focusing on these performance metrics, the algorithm can effectively evaluate and compare different airfoil shapes and configurations, ultimately identifying the most aerodynamically efficient designs that meet the desired criteria.

In future research we will investigate the addition of deflection angle as an additional variable and the application of multi-objective optimization techniques. Furthermore, extending the algorithm's implementation to the leading edge will be explored. These investigations will contribute to a more comprehensive understanding of aerodynamic shape optimization and expand the potential applications of the proposed method.

7. Conclusions

In conclusion, this study demonstrates a novel method for optimizing the aerodynamic shape of the morphing flaps used for compliant morphing structures. The modified finite element method, which incorporated rigid rotation corrections, provides a computationally efficient means of representing airfoil shapes through structural modeling. By incorporating this method into the optimization process, it enables the development of morphing trailing edges while adhering to predefined complaint structure constraints. The effectiveness of adhering to the constraints in the proposed method ensures that the optimized airfoil shape not only achieves improved aerodynamic performance but also maintains the necessary structural integrity and complies with design limitations. In addition to observed improvement in aerodynamic performance demonstrated in the case study, it highlights the potential of this method to be used as a tool for optimizing the shape of morphing flaps.

Author Contributions: Conceptualization, M.L.; methodology, M.L.; software, M.L.; validation, M.L.; formal analysis, M.L.; investigation, M.L.; resources, M.L. and V.L.; data curation, M.L. and V.L.; writing—original draft preparation, M.L. and V.L.; writing—review and editing, M.L. and V.L.; visualization, M.L.; supervision, M.L. and V.L.; project administration, M.L. and V.L. All authors have read and agreed to the published version of the manuscript.

Funding: This research received no external funding.

Institutional Review Board Statement: Not applicable.

Informed Consent Statement: Not applicable.

Data Availability Statement: Not applicable.

Conflicts of Interest: The authors declare no conflict of interest.

References

1. Fujiwara, G.E.; Nguyen, N.T.; Livne, E.; Bragg, M.B. Aerostructural Design Optimization of a Flexible Wing Aircraft with Continuous Morphing Trailing Edge. In Proceedings of the 2018 Multidisciplinary Analysis and Optimization Conference, Atlanta, GA, USA, 25–29 June 2018. [CrossRef]
2. Watkins, J.; Bouferrouk, A. The Effects of a Morphed Trailing-Edge Flap on the Aeroacoustic and Aerodynamic Performance of a 30P30N Aerofoil. *Acoustics* **2022**, *4*, 248–267. [CrossRef]
3. Majid, T.; Jo, B.W. Comparative Aerodynamic Performance Analysis of Camber Morphing and Conventional Airfoils. *Appl. Sci.* **2021**, *11*, 10663. [CrossRef]
4. Masters, D.; Taylor, N.J.; Rendall, T.; Allen, C.; Poole, D. Geometric Comparison of Aerofoil Shape Parameterization Methods. *AIAA J.* **2017**, *55*, 1575–1589. [CrossRef]
5. Sripawadkul, V.; Padulo, M.; Guenov, M. A Comparison of Airfoil Shape Parameterization Techniques for Early Design Optimization. In Proceedings of the 13th AIAA/ISSMO Multidisciplinary Analysis and Optimization Conference, Fort Worth, TX, USA, 13–15 September 2010. [CrossRef]
6. Hoyos, J.; Jímenez, J.H.; Echavarría, C.; Alvarado, J.P. Airfoil Shape Optimization: Comparative Study of Meta-heuristic Algorithms, Airfoil Parameterization Methods and Reynolds Number Impact. *IOP Conf. Ser. Mater. Sci. Eng.* **2021**, *1154*, 012016. [CrossRef]
7. Sobieczky, H. Parametric Airfoils and Wings. In *Recent Development of Aerodynamic Design Methodologies*; Notes on Numerical Fluid Mechanics (NNFM); Fujii, K., Dulikravich, G.S., Eds.; Vieweg + Teubner Verlag: Cham, Switzerland, 1999; Volume 65. [CrossRef]
8. Kulfan, B.M. Universal Parametric Geometry Representation Method. *J. Aircr.* **2008**, *45*, 142–158. [CrossRef]
9. He, W.; Liu, X. Improved aerofoil parameterisation based on class/shape function transformation. *Aeronaut. J.* **2019**, *123*, 310–339. [CrossRef]
10. Zhu, F.; Qin, N. Intuitive Class/Shape Function Parameterization for Airfoils. *AIAA J.* **2014**, *52*, 17–25. [CrossRef]
11. Christie, R.; Robinson, M.; Tejero, F.; MacManus, D.G. The use of hybrid intuitive class shape transformation curves in aerodynamic design. *Aerosp. Sci. Technol.* **2019**, *95*, 105473. [CrossRef]
12. Deng, F.; Xue, C.; Qin, N. Parameterizing Airfoil Shape Using Aerodynamic Performance Parameters. *AIAA J.* **2022**, *60*, 4399–4412. [CrossRef]
13. Ahmad, D.; Ajaj, R.M. A Multiaxial Fracture of Ecoflex Skin with Different Shore Hardness for Morphing Wing Application. *Polymers* **2023**, *15*, 1526. [CrossRef]

14. Bishay, P.L.; Kok, J.S.; Ferrusquilla, L.J.; Espinoza, B.M.; Heness, A.; Buendia, A.; Zadoorian, S.; Lacson, P.; Ortiz, J.D.; Basilio, R.; et al. Design and Analysis of MataMorph-3: A Fully Morphing UAV with Camber-Morphing Wings and Tail Stabilizers. *Aerospace* **2022**, *9*, 382. [CrossRef]
15. Mahid, N.M.; Woods, B.K.S. Initial exploration of a compliance-based morphing fairing concept for hinged aerodynamic surfaces. *Aerosp. Sci. Technol.* **2023**, *136*, 108244. [CrossRef]
16. Kölbl, M.; Ermanni, P. Structural design and analysis of an anisotropic, bi-axially morphing skin concept. *Aerosp. Sci. Technol.* **2022**, *120*, 107292. [CrossRef]
17. Zhang, Y.; Ge, W.; Zhang, Z.; Mo, X.; Zhang, Y. Design of compliant mechanism-based variable camber morphing wing with nonlinear large deformation. *Int. J. Adv. Robot. Syst.* **2019**, *16*. [CrossRef]
18. Taguchi, K.; Fukunishi, K.; Takazawa, S.; Sunada, Y.; Imamura, T.; Rinoie, K.; Yokozeki, T. Experimental Study about the Deformation and Aerodynamic Characteristics of the Passive Morphing Airfoil. *Trans. Jpn. Soc. Aeronaut. Space Sci.* **2020**, *63*, 18–23. [CrossRef]
19. Zhang, Z.; Song, C.; Yang, C.; Cavalieri, V.; De Gaspari, A.; Ricci, S. Combining Density-based Approach and Optimization Refinement in the Design of Morphing Airfoil Structures. In Proceedings of the AIAA Scitech 2020 Forum, Orlando, FL, USA, 6–10 January 2020. [CrossRef]
20. Jia, S.; Zhang, Z.; Zhang, H.; Song, C.; Yang, C. Wind Tunnel Tests of 3D-Printed Variable Camber Morphing Wing. *Aerospace* **2022**, *9*, 699. [CrossRef]
21. Mkhoyan, T.; Thakrar, N.R.; De Breuker, R.; Sodja, J. Morphing wing design using integrated and distributed trailing edge morphing. *Smart Mater. Struct.* **2022**, *31*, 125025. [CrossRef]
22. Zhang, Z.; De Gaspari, A.; Ricci, S.; Song, C.; Yang, C. Gradient-Based Aerodynamic Optimization of an Airfoil with Morphing Leading and Trailing Edges. *Appl. Sci.* **2021**, *11*, 1929. [CrossRef]
23. Leal, P.B.C.; Hartl, D.J. Structurally Consistent Class/Shape Transformation Equations for Morphing Airfoils. *J. Aircr.* **2019**, *56*, 505–516. [CrossRef]
24. Da Silva, V.D. *Mechanics and Strength of Materials*; Springer: Berlin/Heidelberg, Germany, 2006; pp. 1–529.
25. Liu, G.R.; Quek, S.S. *The Finite Element Method: A Practical Course*, 2nd ed.; Elsevier: Amsterdam, The Netherlands, 2013; pp. 1–433. [CrossRef]
26. Drela, M. *XFOIL: An Analysis and Design System for Low Reynolds Number Airfoils*; Springer: Berlin/Heidelberg, Germany, 1989; pp. 1–12.
27. Drela, M. Pros & Cons of Airfoil Optimization. *Front. Comput. Fluid Dyn.* **1998**, *1998*, 363–381. [CrossRef]
28. The MathWorks, Inc. *Global Optimization Toolbox User's Guide R2022b*; The MathWorks, Inc.: Natick, MA, USA, 2022; ISBN 252.2277014.
29. Kumar, T.R.S.; Venugopal, S.; Ramakrishnananda, B.; Vijay, S. Aerodynamic Performance Estimation of Camber Morphing Airfoils for Small Unmanned Aerial Vehicle. *J. Aerosp. Technol. Manag.* **2020**, *12*, e1420. [CrossRef]
30. Bashir, M.; Longtin-Martel, S.; Botez, R.; Wong, T. Aerodynamic Design Optimization of a Morphing Leading Edge and Trailing Edge Airfoil–Application on the UAS-S45. *Appl. Sci.* **2021**, *11*, 1664. [CrossRef]
31. Sheikh, H.M.; Lee, S.; Wang, J.; Marcus, P.S. Airfoil Optimization Using Design-by-Morphing. *arXiv* **2022**, arXiv:2207.11448. [CrossRef]
32. Talebitooti, R.; Gohari, H.; Zarastvand, M. Multi objective optimization of sound transmission across laminated composite cylindrical shell lined with porous core investigating Non-dominated Sorting Genetic Algorithm. *Aerosp. Sci. Technol.* **2017**, *69*, 269–280. [CrossRef]

Disclaimer/Publisher's Note: The statements, opinions and data contained in all publications are solely those of the individual author(s) and contributor(s) and not of MDPI and/or the editor(s). MDPI and/or the editor(s) disclaim responsibility for any injury to people or property resulting from any ideas, methods, instructions or products referred to in the content.